

Complex molecules in W51 North region

Jialei Rong^{1*}, Sheng-Li Qin^{1*}, Luis A. Zapata², Yuefang Wu³,
Tie Liu⁴, Chengpeng Zhang³, Yaping Peng¹, Li Zhang¹ and Ying Liu⁵

¹*Department of Astronomy, Yunnan University, and Key Laboratory of Astroparticle Physics of Yunnan Province, Kunming, 650091, China*

²*Centro de Radioastronomía y Astrofísica, Universidad Nacional Autónoma de México, 58089 Morelia, Michoacán, México*

³*Department of Astronomy, Peking University, Beijing, 100871, China*

⁴*Korea Astronomy and Space Science Institute 776, Daedeokdaero, Yuseong-gu, Daejeon, Republic of Korea 305-348*

⁵*Department of Physics and Hebei Advanced film Laboratory, Hebei Normal University, Shijiazhuang 050024, China*

ABSTRACT

We present Submillimeter Array (SMA) molecular line observations in two 2 GHz-wide bands centered at 217.5 and 227.5 GHz, toward the massive star forming region W51 North. We identified 84 molecular line transitions from 17 species and their isotopologues. The molecular gas distribution of these lines mainly peaks in the continuum position of W51 North, and has a small tail extending to the west, probably associated with W51 d2. In addition to the commonly detected nitrogen and oxygen-bearing species, we detected a large amount of transitions of the Acetone (CH_3COCH_3) and Methyl Formate (CH_3OCHO), which may suggest that these molecules are present in an early evolutionary stage of the massive stars. We also found that W51 North is an ethanol-rich source. There is no obvious difference in the molecular gas distributions between the oxygen-bearing and nitrogen-bearing molecules. Under the assumption of Local Thermodynamic Equilibrium (LTE), with the XCLASS tool, the molecular column densities, and rotation temperatures are estimated. We found that the oxygen-bearing molecules have considerable higher column densities and fractional abundances than the nitrogen-bearing molecules. The rotation temperatures range from 100 to 200 K, suggesting that the molecular emission could be originated from a warm environment. Finally, based on the gas distributions, fractional abundances and the rotation temperatures, we conclude that CH_3OH , $\text{C}_2\text{H}_5\text{OH}$, CH_3COCH_3 and $\text{CH}_3\text{CH}_2\text{CN}$ might be synthesized on the grain surface, while gas phase chemistry is responsible for the production of CH_3OCH_3 , CH_3OCHO and CH_2CHCN .

Key words: ISM:abundances — ISM:individual (W51 North) — ISM:molecules — radio lines: ISM — stars:formation

1 INTRODUCTION

There are three promising theoretical models to explain the formation of the massive stars: monolithic collapse, competitive accretion, and mergers of low mass stars (see for a review, Zinnecker & Yorke 2007). However, their relative large distances (a few parsecs), the clustered formation environments, and their short timescales have made extremely difficult to discard any of these models (Zapata et al. 2015).

Massive stars have a substantial impact on their surrounding environments, making important contributions to the chemistry enrichment of the interstellar medium (e. g., Hernández-Hernández et al. 2014). Thus, searching for complex molecules in massive star formation regions is a crucial

building block to understand massive star formation, since these molecules can provide information on the physical conditions and evolutionary phases of massive star formation (Herbst & van Dishoeck 2009).

The W51 North is one of well-studied massive star-forming regions within the luminous cluster W51-IRS2 (Zapata, Tang & Leurini 2010). The distance from W51 North to the Sun is approximately 7 kpc (Imai et al. 2002). However, a more recent and accurate estimation from Xu et al. (2009) obtained $5.1^{+2.9}_{-1.4}$ kpc.

A large number of H_2O and OH masers, bright dust emission, outflows, and infalling gas were observed toward W51 North region, indicating that this region is forming indeed massive stars (Downes et al. 1979; Zhang, Ho & Ohashi 1998; Zapata et al. 2008, 2009; Zapata, Tang & Leurini 2010). Absence of centimeter emission suggests

* E-mail: JiaLeiRong@163.com, slqin@bao.ac.cn

that W51 North may represent an extremely early stage of the massive star formation (Downes et al. 1979; Zhang, Ho & Ohashi 1998). As the Submillimeter Array (SMA¹) has a broad bandwidth (4 GHz, at the time of these observations) one can detect multiple complex molecules simultaneously, allowing to trace the physical and chemical properties of massive star formation environments close to the massive protostars.

In this paper, we present the results from the SMA observations of W51 North region. We have identified 17 species and obtained their physical parameters by the use of XCLASS program. We describe the observations in §2. In §3 we present observational results, followed by data analysis in §4. §5 discusses individual molecules. We summarize the results in §6.

2 OBSERVATIONS

Track-sharing observations toward W51 North and W51 Main sources were carried out with the SMA in 2005 August, using seven antennas in its compact array. The phase-tracking center of W51 north was placed at R.A.=19^h23^m40^s.05, decl.=+14°31′05″.59 (J2000.0). The typical system temperature of 183 K indicates good weather during observations. The observations covered frequencies from 216.5 to 218.5 GHz (lower sideband), and 226.5 to 228.5 GHz (upper sideband) with a frequency resolution of 0.8125 MHz.

The calibration and imaging were done in Miriad. Bandpass ripples were corrected with the QSO 3C454.3 and Uranus. We also corrected baseline-based bandpass errors using the QSO 3C454.3. QSOs 1741-038 and 1749+096 were used for phase calibration. Uranus was used for flux calibration, and the absolute flux scale is estimated to be accurate to within 20%. Continuum subtraction was made in UV domain. Self-calibration was performed to the continuum data, and the gain solutions from the continuum were applied to the line data.

The synthesized beam sizes of the continuum and line images are approximately 3″.1 × 2″.8 (P.A.=79.0°). 1 σ rms noises of the continuum and lines are approximately 0.01 Jy beam⁻¹ and 0.1 Jy beam⁻¹, respectively. 1 Jy beam⁻¹ corresponds to a main beam brightness temperature of 2.7 K.

3 RESULTS

3.1 Continuum

Continuum image was constructed from line-free channels of LSB and USB UV data, as shown in Figure 1. The continuum image shows a compact and strong source at the position of W51 North, with an extension to the north, which embraces IRS2d source. KJD3 and W51d2 are located east and west of W51 North, respectively (Zapata et al. 2008).

Two dimension Gaussian fits were made to the continuum obtaining the peak intensity and total integrated flux of $\sim 3.0 \pm 0.3$ Jy beam⁻¹ and $\sim 6.7 \pm 0.8$ Jy, respectively.

Under the assumptions that an average grain radius is 0.1 μ m, grain density is 3 gr cm⁻³ and a gas to dust ratio is 100, the H₂ column density and mass can be calculated by the formula (Lis, Carlstrom & Keene 1991),

$$N_{H_2} = 8.1 \times 10^{17} \frac{e^{\frac{h\nu}{\kappa T}} - 1}{Q(\nu)\Omega} \left(\frac{S_\nu}{Jy}\right) \left(\frac{\nu}{GHz}\right)^{-3} (cm^{-2}), \quad (1)$$

and

$$M_{H_2} = 1.3 \times 10^4 \frac{e^{\frac{h\nu}{\kappa T}} - 1}{Q(\nu)} \left(\frac{S_\nu}{Jy}\right) \left(\frac{\nu}{GHz}\right)^{-3} \left(\frac{D}{kpc}\right)^2 (M_\odot), \quad (2)$$

where κ and h are Boltzmann constant and Planck constant, respectively. T is the dust temperature, $Q(\nu)$ is the grain emissivity at frequency ν , S_ν is the total integrated flux of the continuum and Ω is the solid angle subtended by the source, D is the distance from the source to Sun.

The CH₃OH is a grain surface molecule. Here, this molecule peaks at the position of the continuum source associated with W51 North (see Figure 3 and discussion in section 5). Probably the dust and gas are well coupled through collisions in W51 North region. So we assumed that the dust temperature equals the rotation temperature of 138 K derived from the CH₃OH lines. We adopt $Q(\nu) = 2.2 \times 10^{-5}$ at 1.3 mm ($\beta = 1.5$) (Lis & Goldsmith 1990; Lis, Carlstrom & Keene 1991). Therefore, we obtained a source-averaged H₂ column density of 6.4×10^{24} cm⁻² and an H₂ mass of $\sim 1348 M_\odot$. As the continuum peaks at W51 North, then the mass estimated from peak intensity should correspond to gas mass of W51 North source. The H₂ mass of $\sim 610 \pm 61 M_\odot$ is estimated from the continuum peak intensity.

A similar result, $\sim 400 M_\odot$ was reported by Zhang, Ho & Ohashi (1998), in which they calculated the mass of W51 North based on a dust temperature of 100 K, continuum peak intensity of ~ 2.0 Jy beam⁻¹ at $\nu \sim 140$ GHz, D of $7 \sim 8$ kpc and $\beta = 1.0$. If we take $\beta = 1.0$, then $Q(\nu) \approx 2.51 \times 10^{-5}$ at 1.3 mm and then the H₂ mass of $\sim 535 \pm 54 M_\odot$ is obtained. A dust temperature larger than 100 K suggests that dust grains are not coagulated with ice mantles, and thus $\beta \sim 1.5$ is a reasonable guess in W51 North (Ossenkopf & Henning 1994). Therefore the difference of mass between ours and $\sim 400 M_\odot$ by Zhang, Ho & Ohashi (1998) may be caused by taking different value of distance, $Q(\nu)$ and uncertain of flux calibration.

3.2 Molecular lines

The Lower Sideband and Upper Sideband spectra extracted from the continuum peak position and related with W51 North, are shown as the black curves in Figure 2. A few CN transitions in the USB show absorption features indicating gas infalling onto continuum core (Zapata et al. 2008). The SiO line in emission is tracing the outflow reported by Zapata et al. (2009).

We identify all the molecular transitions using the XCLASS program². 84 molecular transitions from 17 species and their isotopologues are identified (Figure 2). In this

¹ The Submillimeter Array is a joint project between the Smithsonian Astrophysical Observatory and the Academia Sinica Institute of Astronomy and Astrophysics and is funded by the Smithsonian Institution and the Academia Sinica.

² <http://www.astro.uni-koeln.de/projects/schilke/XCLASS>

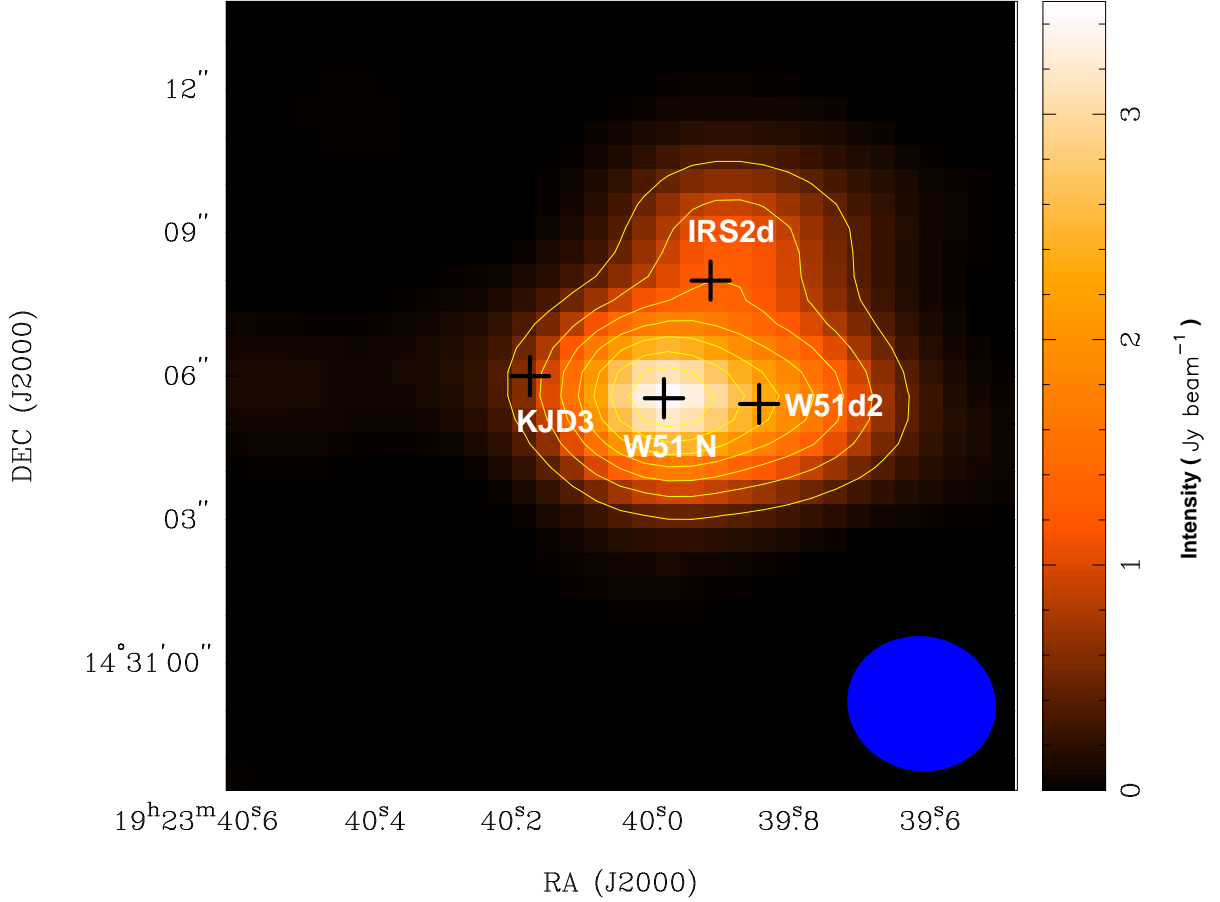


Figure 1. The continuum image at 227 GHz, shown in both contours and grey. The contour levels are 5%, 10%, 20%, 30%, 40%, 50%, 60%, 70%, 80%, 90%, 100% of the maximum intensity of $\sim 3.0 \text{ Jy beam}^{-1}$. The color scale on the right shows the intensity ranging from 0 to 3.5 Jy beam^{-1} . The synthesized beam is shown in the bottom right corner.

image the corresponding molecular names are labelled, including oxygen-bearing molecules of CH_3OH , H_2CO , $\text{C}_2\text{H}_5\text{OH}$, CH_3OCHO , CH_3OCH_3 , CH_3COCH_3 , nitrogen-bearing molecules of CN , $\text{CH}_3\text{CH}_2\text{CN}$, HC_3N , CH_2CHCN , sulfur-bearing molecules of SO_2 , H_2S , SiS , and deuterated molecules of DCN and CH_3CCD . The quantum numbers, frequency, $S_{ij}\mu^2$ and E_u of each transition are summarized in Table 1. Column (1) lists the species and column (2) lists quantum number, column (3), (4) and (5) give frequency, $S_{ij}\mu^2$ and E_u . The source size $\theta_a \times \theta_b$, ΔV and I are given in column (6), (7) and (8), respectively.

3.3 Gas distribution

Figure 3 presents a sample of images from the oxygen-, nitrogen-, and sulfur-bearing molecules, which can provide spatial distribution of specific molecules. In general, all molecular images show a compact structure. The peak emission of the oxygen-bearing molecules of CH_3OH , CH_3COCH_3 and CH_3OCHO , and nitrogen-bearing molecules of CH_2CHCN , $\text{CH}_3\text{CH}_2\text{CN}$ and DCN are coincident with the continuum peak position. The oxygen- and nitrogen-bearing molecules are probably well mixed in

space, which imply that they may have same chemical origin (Remijan et al. 2004). While the emission peak of the sulfur-bearing molecules of H_2S , and SO_2 are located east of the continuum peak. Probably the sulfur-bearing molecules have different chemical routes and form in different environments when compared with the oxygen- and nitrogen-bearing molecules. In addition to the compact source structure, there is an obvious gas extension to the west of the continuum traced by the DCN , H_2S , and SiS is observed.

4 DATA ANALYSIS

The rotation temperatures and fractional abundances of complex molecules can reflect immediate environments close to the stars or star-forming cores, but also can provide key clues in understanding formation mechanism of the specific molecules. In order to obtain reasonable parameters, we use the XCLASS to estimate the column densities and rotation temperatures of the molecules.

Table 1. The molecular line parameters

Molecule	Quantum Numbers	Frequency GHz	$S_{ij}\mu^2$ debye ²	E_u K	$\theta_a \times \theta_b$ arcsec ²	ΔV kms ⁻¹	I Jy/beam
CH ₃ OH	5(1, 4) – 4(2, 2)	216.94556	1.12357	55.87102	3.2×3.0	8.2 ± 0.1	5.0 ± 0.1
	6(1, 5) – 7(2, 6), $v_t = 1$	217.29920	4.66445	373.92517	3.2×3.0	8.6 ± 0.1	3.9 ± 0.1
	15(6, 10) – 16(5, 11), $v_t = 1$	217.64286	4.88652	745.60607	3.2×3.0	8.0 ± 0.2	3.0 ± 0.1
	20(1, 19) – 20(0, 20)	217.88639	11.50535	508.37582	3.2×3.0	8.3 ± 0.2	2.8 ± 0.1
	4(2, 2) – 3(1, 2)	218.44005	3.4766	45.45988	3.2×2.9	8.5 ± 0.1	9.9 ± 0.1
	21(1, 20) – 21(0, 21)	227.09460	11.5939	557.07117	3.1×2.8	7.5 ± 0.2	2.1 ± 0.1
	16(1, 16) – 15(2, 13)	227.81465	5.23842	327.23797	3.0×2.8	7.7 ± 0.1	4.3 ± 0.1
¹³ CH ₃ OH	14(1, 13) – 13(2, 12)	217.04462	5.78629	254.25167	3.2×3.0	5.2 ± 0.4	0.9 ± 0.1
	10(2, 8) – 9(3, 7)	217.39955	2.68164	162.41055	3.2×3.0	4.0 ± 0.9	0.3 ± 0.1
H ₂ CO	3(0, 3) – 2(0, 2)	218.22219	16.30796	20.9564	3.2×2.9	8.4 ± 0.1	11.1 ± 0.1
	3(2, 2) – 2(2, 1)	218.47563	9.06194	68.0937	3.2×2.9	8.0 ± 0.1	7.1 ± 0.1
C ₂ H ₅ OH	8(4, 5) – 7(3, 5)	216.65968	5.00042	106.29995	3.2×3.0	8.5 ± 1.6	0.3 ± 0.1
	5(1, 4) – 4(0, 4)	217.54815	3.63648	75.60201	3.2×3.0	5.9 ± 0.6	0.5 ± 0.1
	5(3, 3) – 4(2, 2)	217.80369	5.98544	23.89298	3.2×3.0	7.3 ± 0.4	1.1 ± 0.1
	5(3, 2) – 4(2, 3)	218.46123	5.59497	23.89375	3.2×2.9	10.5 ± 0.1	4.8 ± 0.1
	26(2, 24) – 26(1, 25)	226.58134	28.24034	304.69227	3.1×2.8	2.0 ± 1.0	0.2 ± 0.1
	10(2, 9) – 9(1, 8)	226.66170	7.05411	51.02783	3.1×2.8	6.4 ± 0.4	1.0 ± 0.1
	13(3, 10) – 12(3, 9)	227.29475	19.66545	148.56961	3.1×2.8	6.7 ± 0.5	0.9 ± 0.1
	18(5, 13) – 18(4, 14)	227.60608	18.61686	175.30421	3.1×2.8	11.2 ± 0.2	3.6 ± 0.1
	3(2, 2) – 2(1, 2)	227.76082	2.02053	71.44923	3.0×2.8	3.6 ± 0.5	0.6 ± 0.1
	13(1, 12) – 12(1, 11)	227.89191	20.6452	140.01443	3.1×2.8	9.0 ± 0.6	0.8 ± 0.1
	13(3, 10) – 12(3, 9)	228.02905	19.66581	143.89662	3.1×2.8	6.1 ± 0.3	1.2 ± 0.1
	11(1, 10) – 10(2, 8)	228.28855	2.47972	118.95090	3.0×2.8	3.9 ± 1.7	0.2 ± 0.1
	7(3, 4) – 7(2, 6)	228.52283	4.05832	95.90890	3.0×2.8	4.5 ± 0.4	0.4 ± 0.1
CH ₃ OCH ₃	22(4, 19) – 22(3, 20) AA	217.19317	162.14491	253.41131	3.2×3.0	6.0 ± 0.3	1.2 ± 0.1
	23(3, 21) – 23(2, 22) AA	218.49503	78.0112	263.83508	3.2×2.9	6.0 ± 0.8	0.5 ± 0.1
	26(5, 21) – 26(4, 22) EA	227.64812	84.89383	355.76623	3.1×2.8	6.0 ± 1.9	0.2 ± 0.1
	24(3, 22) – 24(2, 23) AE	227.65439	78.79933	285.56311	3.1×2.8	4.0 ± 0.5	0.7 ± 0.1
CH ₃ COCH ₃	19(4, 16) – 18(3, 15) EE	217.02251	2042.48098	115.49565	3.2×3.0	6.6 ± 0.2	2.3 ± 0.1
	19(4, 16) – 18(3, 15) AA	217.07050	765.72157	115.43113	3.2×3.0	7.1 ± 0.3	1.5 ± 0.1
	20(2, 18) – 19(3, 17) EA	218.09145	146.20943	119.17572	3.2×2.9	7.5 ± 0.4	1.2 ± 0.1
	20(3, 18) – 19(2, 17) EE	218.12721	1200.40770	119.10113	3.2×2.9	8.3 ± 0.2	2.4 ± 0.1
	20(3, 18) – 19(2, 17) AA	218.16293	1461.76777	119.02728	3.2×2.9	7.1 ± 0.3	1.3 ± 0.1
	12(9, 3) – 11(8, 4) EE	226.81261	547.66326	66.18982	3.2×2.9	7.1 ± 0.3	1.3 ± 0.1
	20(3, 17) – 19(4, 16) AA	226.87939	817.15094	126.31957	3.1×2.8	11.2 ± 2.0	0.3 ± 0.1
	20(3, 17) – 19(4, 16) EE	226.83206	2179.59244	126.38182	3.1×2.8	7.6 ± 0.3	1.5 ± 0.1
	35(10, 26) – 35(9, 27) EE	227.89467	215.20891	418.29082	3.0×2.8	7.3 ± 0.3	1.7 ± 0.1
	21(2, 19) – 20(3, 18) EA	227.90395	619.07570	130.11255	3.0×2.8	7.5 ± 0.3	1.5 ± 0.1
	21(3, 19) – 20(3, 18) EE	227.93937	672.20702	130.04037	3.0×2.8	7.2 ± 0.2	1.9 ± 0.1
	21(2, 19) – 20(3, 18) AA	227.97476	1547.25807	129.96837	3.1×2.8	9.2 ± 0.2	2.2 ± 0.1
	12(10, 3) – 11(9, 2) AE	228.50287	378.05109	68.56948	3.0×2.8	3.3 ± 0.6	0.5 ± 0.1
CH ₃ OCHO	18(2, 16) – 17(2, 15) E	216.83020	46.13641	105.67781	3.2×3.0	7.0 ± 0.1	2.9 ± 0.1
	18(2, 16) – 17(2, 15) A	216.83889	46.14168	105.6673	3.2×3.0	8.6 ± 0.2	2.1 ± 0.1
	20(0, 20) – 19(0, 19) E	216.96625	52.81048	111.49826	3.2×3.0	9.1 ± 0.1	6.0 ± 0.1
	17(4, 13) – 16(4, 12) A	217.31263	42.78270	289.95716	3.2×3.0	6.0 ± 0.6	0.7 ± 0.1
	17(4, 13) – 16(4, 12) E	218.10844	42.94997	289.67911	3.2×3.0	7.7 ± 1.2	0.4 ± 0.1
	17(3, 14) – 16(3, 13) E	218.28090	43.5903	99.72935	3.2×2.9	7.4 ± 0.2	3.0 ± 0.1
	17(3, 14) – 16(3, 13) A	218.29789	43.60233	99.72110	3.2×2.9	11.0 ± 0.3	2.1 ± 0.1
	33(6, 28) – 33(5, 29) A	226.58140	6.87080	357.68199	3.1×2.8	4.1 ± 0.9	0.4 ± 0.1
	20(2, 19) – 19(2, 18) E	226.71306	52.04002	120.22039	3.1×2.8	9.0 ± 0.2	2.1 ± 0.1
	20(2, 19) – 19(2, 18) A	226.71875	51.409	120.207	3.1×2.8	8.5 ± 0.2	2.0 ± 0.1
	20(1, 19) – 19(1, 18) E	226.77315	51.417	120.21536	3.1×2.8	8.9 ± 0.2	2.0 ± 0.1
	20(1, 19) – 19(1, 18) A	226.77879	52.0425	120.20297	3.1×2.8	9.5 ± 0.3	2.0 ± 0.1
	19(2, 17) – 18(2, 16) E	227.01955	48.76106	116.573	3.1×2.8	7.5 ± 0.2	2.1 ± 0.1
	19(2, 17) – 18(2, 16) A	227.02810	48.4690	116.56162	3.1×2.8	8.6 ± 0.2	2.2 ± 0.1
	21(1, 21) – 20(0, 20) E	227.56269	8.88264	122.41946	3.1×2.8	8.5 ± 0.1	6.0 ± 0.1
	18(3, 15) – 17(3, 14) E	228.21129	46.25056	297.16473	3.0×2.8	3.4 ± 1.2	0.9 ± 0.1

Table 1. Continued.

Molecule	Quantum Numbers	Frequency GHz	$S_{ij}\mu^2$ debye ²	E_u K	$\theta_a \times \theta_b$ arcsec ²	ΔV kms ⁻¹	I Jy/beam
DCN	$J = 3 - 2, F = 3 - 2$	217.23855	23.85251	20.85164	3.2×3.0	7.8 ± 0.1	6.1 ± 0.1
CH ₃ CH ₂ CN	24(3, 21) – 23(3, 20)	218.38997	350.22816	139.91753	3.2×2.9	7.0 ± 0.3	1.3 ± 0.1
	25(3, 22) – 24(3, 21)	227.78097	365.32437	150.84922	3.0×2.8	6.0 ± 0.3	1.4 ± 0.1
	25(2, 23) – 24(2, 22)	228.48314	368.05531	146.59165	3.0×2.8	7.0 ± 0.3	1.3 ± 0.1
HC ₃ N	$J = 24 - 23$	218.32479	332.86626	130.98209	3.2×2.9	8.7 ± 0.1	5.7 ± 0.1
	$J = 25 - 24$	227.41891	346.74084	141.89637	3.1×2.8	8.5 ± 0.1	4.9 ± 0.1
HCC ¹³ CN	$J = 24 - 23$	217.41957	334.2359	130.43896	3.2×3.0	3.8 ± 0.7	0.4 ± 0.1
CH ₂ CHCN	23(2, 22) – 22(2, 21)	216.93672	996.36042	133.93474	3.2×3.0	9.0 ± 0.7	0.8 ± 0.1
	23(6, 17) – 22(6, 16)	218.40245	935.94512	203.51934	3.2×2.9	5.5 ± 0.5	0.8 ± 0.1
	23(8, 16) – 22(8, 15)	218.42180	882.77691	263.80899	3.2×2.9	6.2 ± 1.0	0.4 ± 0.1
	23(10, 13) – 22(10, 12)	218.52000	814.48136	341.05429	3.2×2.9	5.3 ± 1.2	0.3 ± 0.1
	24(8, 16) – 23(8, 15)	227.91864	931.50638	274.74733	3.0×2.8	5.7 ± 1.2	0.3 ± 0.1
	24(5, 19) – 23(5, 18)	227.96759	1002.49119	190.73697	3.1×2.8	8.3 ± 0.9	0.5 ± 0.1
	24(3, 22) – 23(3, 21)	228.09054	1031.47311	156.23271	3.0×2.8	9.7 ± 0.8	0.6 ± 0.1
	24(4, 21) – 23(4, 20)	228.10462	1018.75491	171.33742	3.0×2.8	9.7 ± 0.8	0.6 ± 0.1
	24(4, 20) – 23(4, 19)	228.16030	1018.75515	171.34687	3.0×2.8	3.6 ± 1.3	0.2 ± 0.1
CH ₃ CCD	14(3) – 13(3)	218.00760	47.28557	143.50905	3.2×3.0	3.8 ± 0.6	0.4 ± 0.1
	14(2) – 13(2)	218.02754	24.27496	107.38842	3.2×2.9	3.8 ± 0.4	0.7 ± 0.1
	14(0) – 13(0)	218.04350	24.78309	78.48706	3.2×2.9	6.6 ± 0.5	0.7 ± 0.2
SO ₂	22(2, 20) – 22(1, 21)	216.64330	35.25156	248.44117	3.2×2.9	11.4 ± 0.1	5.9 ± 0.1
³³ SO	6(5) – 5(4),	217.82718	10.19653	34.67135	3.2×3.0	9.5 ± 0.4	1.2 ± 0.1
H ₂ S	2(2, 0) – 2(1, 1)	216.71043	2.03714	83.97932	3.2×3.0	9.9 ± 0.1	4.3 ± 0.1
SiS	12 – 11	217.81766	36.12197	67.95393	3.2×3.0	5.1 ± 0.4	0.9 ± 0.1

4.1 XCLASS analysis

The XCLASS accesses the CDMS (Müller et al. 2001, Müller et al. 2005; <http://www.cdms.de>) and JPL to get necessary molecular essential parameters (Pickett et al. 1998; <http://spec.jpl.nasa.gov>). Under the assumption of local thermodynamic equilibrium (LTE), the XCLASS takes source size, beam filling factor, line profile, line blending, background temperature, excitation and opacity into account when solving radiative transfer equation. The detailed fitting functions and modeling procedures are described in papers by Zernickel et al. (2012) and Möller, Endres & Schilke (2015). The source sizes of these species are measured by use of two dimension Gaussian fitting to the gas emission of specific molecule. In the LTE calculation, we fix the line width and peak velocity unchanged, and set different rotation temperatures and column densities to simulate the observed spectra. The reasonable parameters were determined when the simulated spectra have same line profiles as the observed ones (see red curve of Figure 2).

The column densities and rotation temperatures of 17 species and their isotopologues are obtained from our LTE calculation, and the results are summarized in Table 2. Column (1) lists the molecular name, column (2) and (3) present the column density and rotation temperature, respectively.

From Table 2, the rotation temperatures of oxygen-bearing molecules range from 110 to 140 K, while nitrogen-bearing molecules have rotation temperatures ranging from 105 to 140 K, which is consistent with that derived from the transitions of CH₃CN (Zhang, Ho & Ohashi 1998). The similar gas temperatures and distributions between oxygen- and nitrogen-bearing molecules (see §3.3) suggest that oxygen-bearing and nitrogen-bearing molecules are well mixed and originate from the same physical environments. The scenario is inconsistent with the observations toward the massive star-forming regions of Orion-KL and G19.61-0.23, in which nitrogen-bearing molecules have higher temperatures than oxygen-bearing molecules and oxygen- and nitrogen-bearing molecules peak at different positions (Blake et al. 1987; Qin et al. 2010). The sulfur-bearing molecules have gas temperatures ranging from 130 to 180 K. The sulfur-bearing molecules have been proved to be a probe of outflows or shocks. The outflow motions are identified in W51 North region (Zapata et al. 2008). The higher gas temperature of the sulfur-bearing molecules in W51 North may be caused by outflow heating.

There are obvious difference in the column densities between the oxygen-bearing and nitrogen-bearing molecules (see Table 2). The column densities of oxygen-bearing molecules range from 4.3×10^{16} to 2.3×10^{18} cm⁻². While

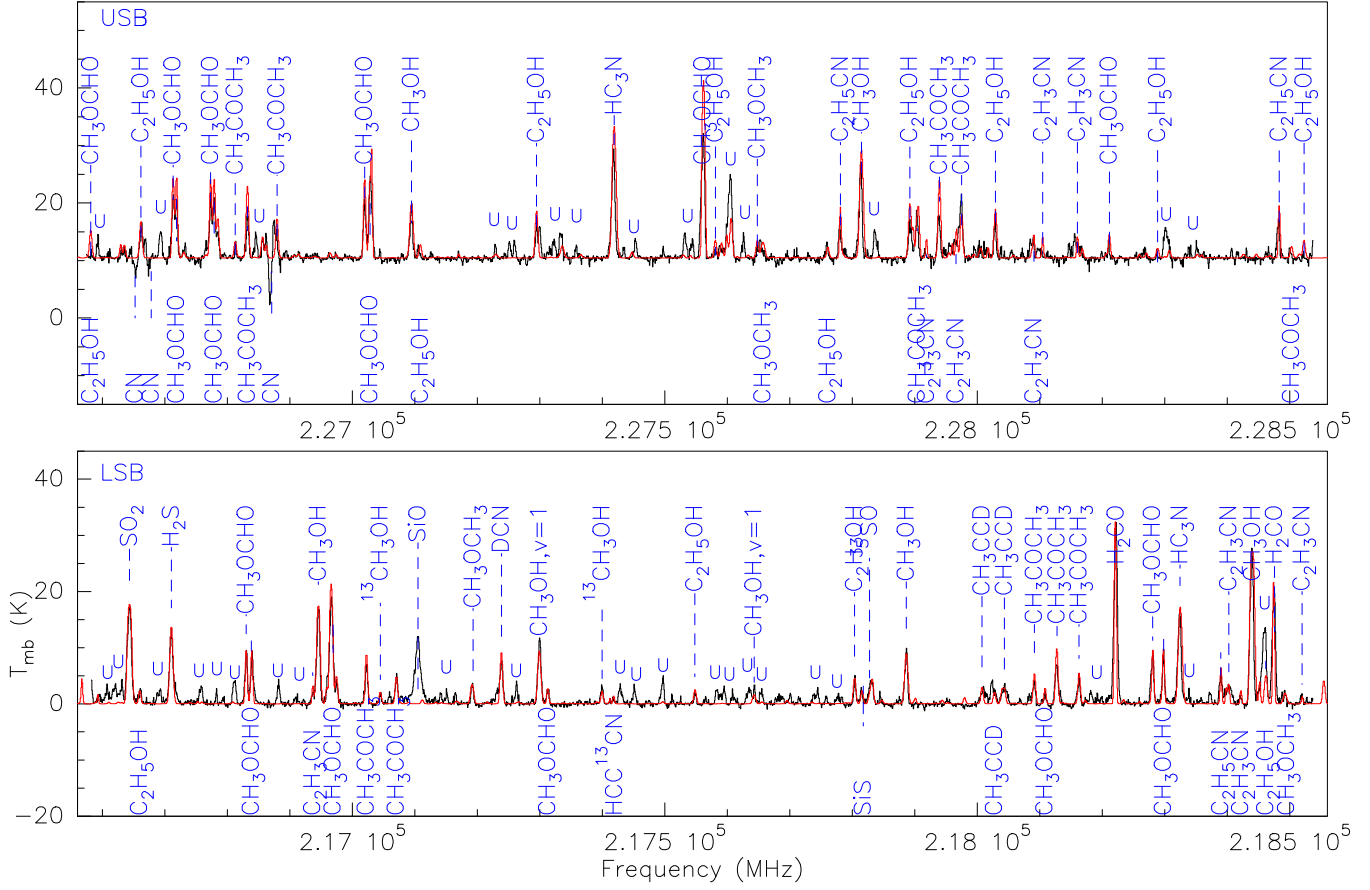


Figure 2. The LSB and USB spectra extracted at the continuum peak position. The black curve is the observed spectra, and red curve indicates simulated spectra using the XCLASS program. U marks the unidentified transitions.

Table 2. The Physical Parameters

Molecule	N (cm^{-2})	T_{rot} (K)	f_{H_2}
CH ₃ OH	2.3×10^{18}	138	3.6×10^{-7}
³ CH ₃ OH	1.1×10^{17}	138	1.7×10^{-8}
C ₂ H ₅ OH	7.4×10^{17}	140	1.2×10^{-7}
CH ₃ OCH ₃	1.8×10^{17}	140	2.8×10^{-8}
CH ₃ COCH ₃	1.4×10^{17}	140	2.2×10^{-8}
H ₂ CO	4.3×10^{16}	110	6.7×10^{-9}
CH ₃ OCHO	3.0×10^{17}	138	4.7×10^{-8}
CH ₂ CHCN	9.2×10^{15}	140	1.4×10^{-9}
CH ₃ CH ₂ CN	2.6×10^{16}	140	4.1×10^{-9}
HC ₃ N	2.8×10^{15}	105	4.4×10^{-10}
HCC ¹³ CN	1.2×10^{14}	105	1.9×10^{-11}
SO ₂	9.4×10^{17}	180	1.5×10^{-7}
³³ SO	3.4×10^{15}	170	5.3×10^{-10}
H ₂ S	4.4×10^{16}	143	6.9×10^{-9}
SiS	1.9×10^{15}	130	3.0×10^{-10}
CH ₃ CCD	6.6×10^{16}	130	1.0×10^{-8}
DCN	6.8×10^{14}	138	1.1×10^{-11}

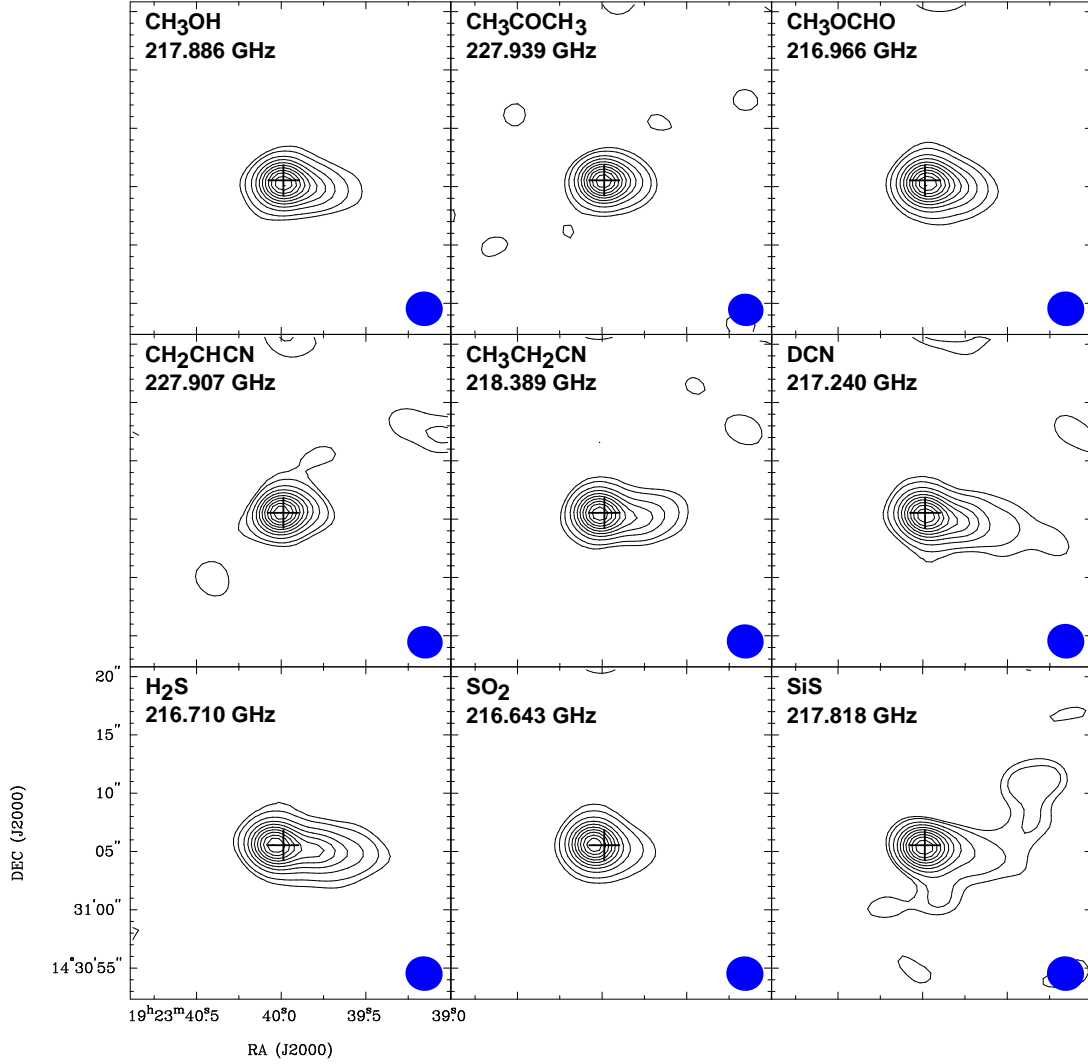


Figure 3. The sample images of specific molecules. In each panel, the synthesized beam is shown in the bottom right corner, the cross symbol marks the continuum peak position. The contour levels are 5%, 10%, 20%, 30%, 40%, 50%, 60%, 70%, 80%, 90%, 100% of the peak value. The peak values of CH_3OH , CH_3COCH_3 , $\text{C}_2\text{H}_5\text{OH}$, CH_2CHCN , $\text{CH}_3\text{CH}_2\text{CN}$, DCN , H_2S , SO_2 and SiS are 24.7, 14.9, 78.6, 15.7, 14.1, 24.3, 45.4, 85.6 and 95.2 Jy beam^{-1} , respectively.

the column densities of the nitrogen-bearing molecules range from 2.8×10^{15} to $2.6 \times 10^{16} \text{ cm}^{-2}$.

4.2 Abundance and isotopic ratio

The fractional abundance of the observed molecules relative to H_2 are estimated by use of the expression, $f_{\text{H}_2} = N_T/N_{\text{H}_2}$, and summarized in column (4) of Table 2, where N_T is column density of specific molecule and N_{H_2} is the column density of H_2 . The oxygen-bearing molecules have relatively higher abundances at a range of 6.7×10^{-9} to 3.6×10^{-7} , while the nitrogen-bearing molecules have abundances ranging from 4.4×10^{-10} to 4.1×10^{-9} . Previous observations of massive star-forming regions also showed that the oxygen-bearing molecules have higher abundances but lower temperatures than the nitrogen-bearing molecules (e. g., Blake et al. 1987; Wyrowski et al. 1999; Qin et

al. 2010). The chemical model proposed by Rodgers & Charnley (2001) suggested that hot-core composition (O-rich or N-rich) depends on core temperature and the ammonia/methanol ratio of the evaporated ices, and the timescale of the core formation, in which O-rich cores form first, then become N-rich as temperature rises and evolution. In our case, the oxygen- and nitrogen-bearing molecules peak at same position and have similar temperature, which may be caused by the fact that W51 North is at an early evolutionary stage and the hot core is not very developed, as suggested by dynamical analysis (Zhang, Ho & Ohashi 1998; Zapata et al. 2008, 2009; Zapata, Tang & Leurini 2010).

The CH_3OH , HC_3N and their isotopologues $^{13}\text{CH}_3\text{OH}$, HCC^{13}CN are detected in W51 North. $^{12}\text{C}/^{13}\text{C}$ ratios of 21.0 and 23.3 are estimated from $\text{CH}_3\text{OH}/^{13}\text{CH}_3\text{OH}$ and $\text{HC}_3\text{N}/\text{HCC}^{13}\text{CN}$, respectively. Based on the relationship of isotope ratios and distance from the Galactic center by

Willson & Rood (1994), the $^{12}\text{C}/^{13}\text{C}$ ratio of 22 is obtained if one takes the distance of 1.5 kpc to the Galactic center. The consistent $^{12}\text{C}/^{13}\text{C}$ ratio from the two methods suggest that the parameters derived from the XCLASS modeling are reasonable.

5 INDIVIDUAL MOLECULES

5.1 Methanol (CH_3OH)

Methanol (CH_3OH) is a key molecule in the chemical networks linked with the formation of more complex oxygen-bearing organic molecules (Bottinelli et al. 2007; Whittet et al. 2011). Five rotational transitions of methanol have been identified in our observations spanning an upper level energies of 45 – 557 K. In addition, we have detected two transitions of CH_3OH from vibrational state at frequencies 217.29920 and 217.64286 GHz with upper level energies of 374 and 746 K, respectively. The CH_3OH has highest fractional abundance of 3.6×10^{-7} than other molecules. Higher CH_3OH abundance is also observed in other massive star-forming regions (e. g., Qin et al. 2010, 2015; Neill et al. 2014). The higher CH_3OH abundance of $\sim 10^{-7}$ can not be explained by gas-phase chemical model (Lee, et al. 1996). The gas-phase chemical model suggested that CH_3OH can be produced in gas phase via radiative association of CH_3^+ and H_2O at temperature ≤ 100 K, giving CH_3OH abundance of $\sim 10^{-11}$ (Lee et al. 1996). In contrast, the grain chemical model suggested that CH_3OH is formed on grain surface via hydrogenation of CO, followed with evaporating from grain surface into gas phase due to temperature increasing, which can produce higher CH_3OH abundances. The higher abundance of $\sim 10^{-7}$ in our observations favor that this molecule originates from grain surface chemistry (Charnley et al. 2004; Garrod & Herbst 2006).

5.2 Acetone (CH_3COCH_3)

Acetone (CH_3COCH_3) had been detected for the first time by Combes et al. (1987) and later confirmed by Snyder et al. (2002). So far acetone (CH_3COCH_3) was only detected in the hot molecular core Sgr B2(N) (Snyder et al. 2002), the Orion KL hot core (Friedel et al. 2005; Peng et al. 2013), and G24.78+0.08 (Codella et al. 2013). We have identified 13 transitions of CH_3COCH_3 in W51 North region, spanning a wide energy range of 66 – 418 K. The column density of $1.4 \times 10^{17} \text{ cm}^{-2}$ and gas temperature of 140 K are estimated by use of the XCLASS, and the higher abundance of 2.0×10^{-8} is obtained.

Combes et al. (1987) proposed that CH_3COCH_3 is formed in gas-phase via the radiative association reaction. However Herbst, Giles & Smith (1990) argued that this radiative association reaction is very inefficient to produce observed CH_3COCH_3 abundance, and this process can only explain the lower abundance of $\sim 10^{-11}$. Recently, the observations of CH_3COCH_3 toward the Orion-KL have shown that the distribution of CH_3COCH_3 is similar to N-bearing molecules concentrated at the hot core rather than O-bearing molecules peaked at the Compact ridge, therefore the formation of CH_3COCH_3 may invoke N-bearing molecules, and grain surface chemistry or high temperature

gas-phase chemistry may play important roles (Friedel et al. 2005, 2008; Peng et al. 2013). The well mixed nitrogen- and oxygen-bearing molecules based on gas distributions and temperatures in W51 North indicate that the hot core is not very developed in W51 North and grain surface chemistry and evaporating from grain surface into gas phase may be responsible for the high CH_3COCH_3 abundance of 2.0×10^{-8} , since the gas temperature is not so high in W51 North.

Compared to the Sgr B2(N) (Snyder et al. 2002), the Orion-KL (Peng et al. 2013), and G24.78+0.08 (Codella et al. 2013) molecule line cores, W51 North region has higher CH_3COCH_3 abundance. The CH_3COCH_3 can be destructed in gas phase by efficient radiative association of H_3^+ and CH_3COCH_3 or the collisions of CH_3COCH_3 and C^+ (Combes et al. 1987; Herbst, Giles & Smith 1990). A possible interpretation of higher CH_3COCH_3 abundance is that unlike the Sgr B2(N), the Orion-KL, and G24.78+0.08, W51 North is at very early stage of massive star formation, and the CH_3COCH_3 is destructed less and converted into the other molecules in a short time.

5.3 Ethanol ($\text{C}_2\text{H}_5\text{OH}$)

We have identified 13 transitions of $\text{C}_2\text{H}_5\text{OH}$ in W51 North region. These transitions have a wide spread of the upper level energies of 23 – 305 K. The $\text{C}_2\text{H}_5\text{OH}$ has higher abundance of 1.2×10^{-7} in our observations. Compared to other sources, the $\text{C}_2\text{H}_5\text{OH}$ abundance of 1.2×10^{-7} and $N_{\text{C}_2\text{H}_5\text{OH}}/N_{\text{CH}_3\text{OH}} \approx 0.32$ are much higher than those in other massive star-forming regions (Ohishi et al. 1995; Qin et al. 2010; Bisschop et al. 2007). Hence W51 North is a very ethanol-rich source.

The gas-phase chemical reaction via ion-molecule reaction predicted $\text{C}_2\text{H}_5\text{OH}$ abundance of $\leq 10^{-11}$ (Leung, Herbst & Huebenr 1984). Higher abundance of 1.2×10^{-7} in our observations can't be explained by pure gas-phase chemical model. The grain chemistry suggested that $\text{C}_2\text{H}_5\text{OH}$ can be formed on the grain surface via hydrogenation of CH_3CO (Charnley et al. 2004; Ohishi et al. 1995), and the model predicted high $\text{C}_2\text{H}_5\text{OH}$ abundance of $10^{-8} \sim 10^{-7}$ within $\sim 10^4$ yr after evaporated from the grain surface into gas phase. Our result appears to support that the $\text{C}_2\text{H}_5\text{OH}$ is synthesized on grain surface (Ohishi et al. 1995; Charnley et al. 1995).

5.4 Dimethyl ether (CH_3OCH_3) and Methyl formate (CH_3OCHO)

Four transitions of CH_3OCH_3 are detected in W51 North. We estimated its rotation temperature of 140 K and column density of $1.8 \times 10^{17} \text{ cm}^{-2}$ from the XCLASS calculation. The abundance ratio of $N_{\text{CH}_3\text{OCH}_3}/N_{\text{C}_2\text{H}_5\text{OH}}$ is approximately 0.24. The $N_{\text{CH}_3\text{OCH}_3}/N_{\text{C}_2\text{H}_5\text{OH}}$ ratios have a great deal of changes from source to source (Fontani et al. 2007; Qin et al. 2010; Millar et al. 1988; Schilke et al. 1997; Bisschop et al. 2007). Although CH_3OCH_3 is isomer of $\text{C}_2\text{H}_5\text{OH}$, the abundances of $\text{C}_2\text{H}_5\text{OH}$ and CH_3OCH_3 are not well correlation, suggesting that they have different chemical route, and do not have same 'parent' molecules.

As one of large oxygen-bearing molecules, CH_3OCHO has been reported in many hot molecular cores and corinos (Blake et al. 1987; Hatchell et al. 1998; Nummelin et

al. 2000; Cazaux et al. 2003; Bottinelli et al. 2004). Sixteen transitions of CH_3OCHO are identified in W51 North, spanning a upper energy level range of 100 – 358 K. High fractional abundance of 4.7×10^{-8} is obtained. Gas temperature, column density and spatial distribution of CH_3OCHO are similar to those of CH_3OCH_3 (see Table 2 and Figure 3). Similar case is also seen in Orion-KL, in which the distributions of CH_3OCHO and CH_3OCH_3 present a striking similarity, and the two species have comparable gas temperature and column density (Brouillet et al. 2013), suggesting that CH_3OCHO and CH_3OCH_3 may be chemically related and have similar formation mechanism (Brouillet et al. 2013).

Charnley, Tielens & Millar (1992) proposed that CH_3OCH_3 and CH_3OCHO can be formed in gas phase chemistry via molecule-ion reaction of CH_3OH_2^+ with CH_3OH and H_2CO , respectively. Their model predicted high abundance of $\sim 10^{-8}$ for CH_3OCH_3 and CH_3OCHO at age of $\sim 10^4$ yr. Our results appear to favor the gas-phase formation routes of CH_3OCH_3 and CH_3OCHO by Charnley, Tielens & Millar (1992).

5.5 Vinyl cyanide (CH_2CHCN) and Ethyl cyanide ($\text{CH}_3\text{CH}_2\text{CN}$)

We have identified 9 CH_2CHCN transitions with upper level energies E_u of 134 – 341 K. The column density of $9.2 \times 10^{15} \text{ cm}^{-2}$ and the rotation temperature of 140 K are obtained. Three $\text{CH}_3\text{CH}_2\text{CN}$ transitions with upper level energies E_u of 139 – 151 K are identified. The column density of $2.6 \times 10^{16} \text{ cm}^{-2}$ and rotation temperature of 140 K are estimated by use of the XCLASS.

CH_2CHCN and $\text{CH}_3\text{CH}_2\text{CN}$ have same temperature of 140 K, while $\text{CH}_3\text{CH}_2\text{CN}$ has higher column density than CH_2CHCN . Previous observations suggested that the abundances of two molecules are strongly correlated (Fontani et al. 2007). $N_{\text{CH}_2\text{CHCN}}/N_{\text{CH}_3\text{CH}_2\text{CN}}$ in W51 North is approximate 0.35 which agrees well with abundance correlation of $\text{CH}_3\text{CH}_2\text{CN}$ and CH_2CHCN in other star-forming regions (Fontani et al. 2007) and CH_2CHCN may be formed through gas phase reactions involving $\text{CH}_3\text{CH}_2\text{CN}$ (Caselli, Hasegawa & Herbst 1993). While $\text{CH}_3\text{CH}_2\text{CN}$ can be formed by successive hydrogenation of HC_3N on dust grains and released into the gas phase as temperature rises (Blake et al. 1987; Caselli, Hasegawa & Herbst 1993). The ratio of $N_{\text{CH}_3\text{CH}_2\text{CN}}/N_{\text{HC}_3\text{N}} \approx 10$ in our observations is consistent with the model prediction of grain surface chemistry (Blake et al. 1987).

5.6 Deuterated molecules

We have detected one transition of the deuterated species of hydrogen cyanide (DCN), in W51 North. The column density of $6.8 \times 10^{14} \text{ cm}^{-2}$ is estimated, which is much larger than those in other sources associated with UC HII regions (Hatchell, Millar & Rodgers 1998). The deuterated species are thought to be synthesized at the early evolutionary stage of star formation (Miettinen, Hennemann & Linz 2011). Previous studies suggested that DCN can be formed via D-H substitution of the HCN or the reaction of CHD with N on the grain mantles and then be released into the gas-phase, while DCN can be destroyed with temperature increasing

(Schilke et al. 1992; Hatchell, Millar & Rodgers 1998). Hence the larger abundance observed in W51 North is not a surprise and suggests that it may be synthesized at the early evolutionary stages of star formation.

As isotopomer of methyl acetylene CH_2DCCH has been reported in the dark cloud TMC-1 CP by Gerin et al. (1992), and CH_3CCD had been successfully detected in same region by Markwick et al. (2005). So far the CH_3CCD has been less reported in other massive star formation regions. Therefore CH_3CCD is an important molecule for investigating the difference of physical and chemical environments between the dark clouds and hot molecular cores. We have successfully identified 3 transitions of CH_3CCD with E_u ranging from 78 to 143 K. Higher CH_3CCD abundance of 1×10^{-8} and temperature of 130 K compared to dark clouds (Markwick et al. 2005) are estimated, which may indicate that CH_3CCD is synthesized on grain surface and release to gas phase as temperature increases.

5.7 Silicon monosulfide (SiS)

One transition of SiS ($J=12-11$) at 217.81766 GHz is identified, and the estimated column density and abundance are $1.9 \times 10^{15} \text{ cm}^{-2}$ and 3.0×10^{-10} , respectively. So far this species is only detected in carbon star IRC+10216, Sgr B2(N), Sgr B2(M) and Sgr B2(OH) (Bieging & Nguyen 1989; Turner 1991; Belloche et al. 2013). The column density of $1.9 \times 10^{15} \text{ cm}^{-2}$ is higher than $\sim 10^{13} \text{ cm}^{-2}$ in Sgr B2. While the fractional abundance of 3.0×10^{-10} in W51 North is lower than $\sim 10^{-6}$ in the carbon star, IRC+10216. The abundance difference of four order of magnitude may be caused by the different physical and chemical environments in massive star formation regions and the asymptotic giant branch star.

5.8 Sulfur-bearing molecules

Sulfur-bearing molecules of H_2S and SO_2 are observed in W51 North, with higher gas temperature than other molecules. The fractional abundances of SO_2 and H_2S are 1.5×10^{-7} and 6.9×10^{-9} , respectively. The ratio of $N_{\text{H}_2\text{S}}/N_{\text{SO}_2}$ is appropriately 0.05, which is same order of magnitude as those in massive protostar cores (Herpin et al. 2009), which is consistent with chemical model that H_2S can be formed on the grain surface and H_2S is converted to SO first, then the SO is converted to SO_2 as temperature rises (Charnley 1997; Wakelam et al. 2004; Woods et al. 2015).

6 SUMMARY

We present the Submillimeter Array (SMA) observations of molecular lines in two 2 GHz-wide bands centered at 217.5 and 227.5 GHz, toward massive star forming region W51 North. We identified 84 transitions from 17 species, including oxygen-, nitrogen- and sulfur-bearing molecules. Our main conclusions are as follows:

1. The gas distributions of both oxygen-bearing and nitrogen-bearing molecules show a compact core concentrated on the strongest continuum source, which indicates that nitrogen- and oxygen-bearing molecules are well-mixed

in space in W51 North region.

2. Under the assumption of local thermodynamic equilibrium, the molecular rotation temperatures and column densities are estimated by use of the XCLASS program. The oxygen-bearing molecules have higher fractional abundance than the nitrogen-bearing molecules. The rotation temperatures range from 100 to 200 K, suggesting that the molecular emissions originate from warm environments.

3. Thirteen transitions of CH_3COCH_3 are identified. Higher fractional abundance of CH_3COCH_3 are obtained in W51 North when compared to the other massive star-forming regions, *e.g.* Sgr B2(N), Orion KL, G24.78+0.08. These results seem to indicate that CH_3COCH_3 is synthesized on grain surface at the early evolutionary stage of massive star formation.

4. Higher fractional abundance of CH_3OH and $\text{C}_2\text{H}_5\text{OH}$ are obtained, which cannot explained by gas phase reactions and the two molecules may be synthesized on grain surface. $N_{\text{C}_2\text{H}_5\text{OH}}/N_{\text{CH}_3\text{OH}} \approx 0.32$ are much higher than those in other massive star-forming regions, and W51 North is a very ethanol-rich source.

5. Similar gas distribution, rotation temperature and abundance between CH_3OCHO and CH_3OCH_3 suggest that they may be chemically related and have similar formation mechanism. The two molecules may originate from gas phase chemistry.

6. $N_{\text{CH}_2\text{CHCN}}/N_{\text{CH}_3\text{CH}_2\text{CN}}$ in W51 North agrees well with abundance correlation of $\text{CH}_3\text{CH}_2\text{CN}$ and CH_2CHCN in other star-forming regions. $\text{CH}_3\text{CH}_2\text{CN}$ can be formed by successive hydrogenation of HC_3N on dust grains while CH_2CHCN may be formed through gas phase reactions involving $\text{CH}_3\text{CH}_2\text{CN}$.

7. CH_3CCD and SiS have been less reported in other star-forming regions. Higher fractional abundances of CH_3CCD and SiS are estimated in W51 North region.

ACKNOWLEDGMENTS

We thank the anonymous referee, and editor Morgan Hollis for their constructive comments on the paper. This work has been supported by the National Natural Science Foundation of China under grant Nos. 11373026, 11373009, 11433004, 11433008, U1331116, and the National Basic Research Program of China (973 Program) under grant No. 2012CB821800, by Top Talents Program of Yunnan Province and Midwest universities comprehensive strength promotion project (XT412001, Yunnan university).

REFERENCES

Belloche A., Müller H. S. P., Menten K. M., Schilke P., Comito, C., 2013, A&A, 559, A47
Bieging J. H., Nguyen Q. -R., 1989, ApJ, 343, L25

Bisschop S. E., Fuchs G. W., van Dishoeck E. F., Linnartz H., 2007, A&A, 474, 1061
Blake G. A., Sutton E. C., Masson C. R., Phillips T. G., 1987, ApJ, 315, 621
Bottinelli S., Boogert A. C. A., van Dishoeck E. F., Oberg K., Pontoppidan K. M., Blake G. A., Evans N. J., Lahuis F., 2007, msl, confE, 11
Bottinelli S. et al., 2004, ApJ, 615, 354
Brouillet N. et al., 2013, A&A, 550, A46
Caselli P., Hasegawa T. I., Herbst E., 1993, ApJ, 408, 548
Cazaux S., Tielens A. G. G. M., Ceccarelli C., Castets A., Wakelam V., Caux E., Parise B., Teyssier D., 2003, ApJ, 593, L51
Charnley S. B., Kress M. E., Tielens A. G. G. M., Millar T. J., 1995, ApJ, 448, 232
Charnley S. B., 1997, ApJ, 481, 396
Charnley S. B., Ehrenfreund P., Millar T. J., Boogert A. C. A., Markwick A. J., Butner H. M., Ruiterkamp R., Rodgers S. D., 2004, MNRAS, 347, 157
Charnley S. B., Tielens A. G. G. M., Millar T. J., 1992, ApJ, 399, L71
Codella C., Beltrán M. T., Cesaroni R., Moscadelli L., Neri R., Vasta M., Zhang Q., 2013, A&A, 550, A81
Combes F., Gerin M., Wootten A., Wlodarczak G., Clauset F., Encrenaz P. J., 1987, A&A, 180, L13
Downes D., Genzel R., Moran J. M., Johnston K. J., Matveenko L. I., Kogan L. R., Kostenko V. I., Ronnang B., 1979, A&A, 79, 233
Fontani F., Pascucci I., Caselli P., Wyrowski F., Cesaroni R., Walmsley C. M., 2007, A&A, 470, 639
Friedel D. N., Snyder L. E., 2008, ApJ, 672, 962
Friedel D. N., Snyder L. E., Remijan A. J., Turner B. E., 2005, ApJ, 632, 95
Garrod R. T., Herbst E., 2006, A&A, 457, 927
Gerin M., Combes F., Wlodarczak G., Encrenaz P., Laurent C., 1992, A&A, 253, L29
Hatchell J., Millar T. J., Rodgers S. D., 1998, A&A, 332, 695
Hatchell J., Millar T. J., Thompson M. A., Macdonald G., 1998, A&AS, 133, 29
Herbst E., Giles K., Smith D., 1990, ApJ, 358, 468
Herbst E., van Dishoeck E. F., 2009, ARA&A, 47, 427
Hernández-Hernández V., Zapata L. A., Kurtz S., Garay G., 2014, ApJ, 786, 38
Herpin F., Marseille M., Wakelam V., Bontemps S., Lis D. C., 2009, A&A, 504, 853
Imai H., Sasao T., Kameya O., Watanabe T., Omodaka T., Nishio M., Asaki Y., Nakajima J., 2002, IAUS, 206, 88
Lee H. -H., Herbst E., Pineau des Forets G., Roueff E., Le Bourlot J., 1996, A&A, 311, 690
Leung C. M., Herbst E., Huebner W. F., 1984, ApJS, 56, 231
Lis D. C., Carlstrom J. E., Keene J., 1991, ApJ, 380, 429
Lis D. C., Goldsmith P. F., 1990, ApJ, 356, 195
Markwick A. J., Charnley S. B., Butner H. M., Millar T. J., 2005, ApJ, 627, L117
Miettinen O., Hennemann M., Linz H., 2011, A&A, 534, A134
Millar T. J., Brown P. D., Olofsson H., Hjalmarsen A., 1988, A&A, 205, L5
Möller, T., Endres, C., & Schilke, P. 2015, accepted by A&A

- Müller H. S. P., Schlöder F., Stutzki J., Winnewisser G., 2005, *JMoSt*, 742, 215
- Müller H. S. P., Thorwirth S., Roth D. A., Winnewisser G., 2001, *A&A*, 370, L49
- Neill J. L. et al., 2014, *ApJ*, 789, 8
- Nummelin A., Bergman P., Hjalmarsen Å., Friberg P., Irvine W. M., Millar T. J., Ohishi M., Saito S., 2000, *ApJS*, 128, 213
- Ohishi M., Ishikawa S. -I., Yamamoto S., Saito S., Amano T., 1995, *ApJ*, 446, L43
- Ossenkopf, V., & Henning, T. 1994, *A&A*, 291, 943
- Peng T. -C. et al., 2013, *A&A*, 554, A78
- Pickett H. M., Poynter R. L., Cohen E. A., Delitsky M. L., Pearson J. C., Müller H. S. P., 1998, *JQSRT*, 60, 883
- Qin S. -L., Schilke P., Wu J. W., Wu Y. F., Liu T., Liu Y., Sánchez-Monge Á., 2015, *ApJ*, 803, 39
- Qin S. -L., Wu Y. F., Huang M. H., Zhao G., Li D., Wang J. -J., Chen S., 2010, *ApJ*, 711, 399
- Remijan A., Shiao Y. -S., Friedel D. N., Meier D. S., Snyder L. E., 2004, *ApJ*, 617, 384
- Rodgers S. D., Charnley S. B., 2001, *APJ*, 546, 324
- Schilke P., Walmsley C. M., Pineau Des Forets G., Roueff E., Flower D. R., Guilloteau S., 1992, *A&A*, 256, 595
- Schilke P., Groesbeck T. D., Blake G. A., Phillips T. G., 1997, *ApJS*, 108, 301
- Snyder L. E., Lovas F. J., Mehringer D. M., Miao N. Y., Kuan Y. -J., Hollis J. M., Jewell P. R., 2002, *ApJ*, 578, 245
- Turner B. E., 1991, *ApJS*, 76, 617
- Wakelam V., Caselli P., Ceccarelli C., Herbst E., Castets A., 2004, *A&A*, 422, 159
- Whittet D. C. B., Cook A. M., Herbst E., Chiar J. E., Shenoy S. S., 2011, *ApJ*, 742, 28
- Wilson T. L., Rood R., 1994, *ARA&A*, 32, 191
- Woods P. M., Occhiogrosso A., Viti S., Kaňuchová Z., Palumbo M. E., Price S. D., 2015, *MNRAS*, 450, 1256
- Wyrowski F., Schilke P., Walmsley C. M., Menten K. M., 1999, *ApJ*, 514, L43
- Xu, Y., Reid, M. J., Menten, K. M., et al. 2009, *ApJ*, 693, 413
- Zapata L. A., Ho P. T. P., Schilke P., Rodríguez L. F., Menten K., Palau A., Garrod R. T., 2009, *ApJ*, 698, 1422
- Zapata L. A., Palau A., Ho P. T. P., Garrod R. T., Rodríguez L. F., Menten K., 2008, *A&A*, 479, L25
- Zapata L. A., Tang Y. -W., Leurini S., 2010, *ApJ*, 725, 1091
- Zapata, L. A., Palau, A., Galván-Madrid, R., et al. 2015, *MNRAS*, 447, 1826
- Zernickel, A., Schilke, P., Schmiedeke, A., et al. 2012, *A&A*, 546, 87
- Zinnecker H., Yorke H. W., 2007, *ARA&A*, 45, 481
- Zhang Q. Z., Ho P. T. P., Ohashi N., 1998, *ApJ*, 494, 636